Cone-Derived Waveriders with Longitudinal Curvature

M.L. Rasmussen* and L.W. Clement†
University of Oklahoma, Norman, Oklahoma

Lifting-body waverider configurations with longitudinal curvature are derived by means of known flowfields past ogival bodies. The flowfields are generated by means of perturbations of the supersonic flow past a circular cone. Approximate analytical solutions for the shock-layer flowfield are found within the framework of hypersonic small-disturbance theory. Perturbations due to longitudinal curvature produce reduced drag, increased lift-to-drag ratios, and provide design advantages for a more efficient volume distribution related to packaging of guidance, propulsion, and payload units.

Nomenclature

A_b = base area of waverider
C_p = pressure coefficient
D = drag
f = body perturbation function
G_m = shock perturbation function for power law
g = shock perturbation function
K_δ = $M_\infty \delta$, hypersonic similarity parameter; δ in radians
L = lift
ℓ = length of basic cone
M_∞ = freestream Mach number
m = perturbation index factor
q = $\rho_\infty V_\infty^2/2$
r = radial distance from vertex
S = projected planform area
S_w = forebody wetted area
V = volume of waverider or fluid velocity
V_∞ = freestream velocity
β = basic-shock semivertex angle
γ = ratio of specific heats
δ = basic-cone semivertex angle
ϵ = small perturbation parameter
Θ = polar angle, measured from z axis
Θ_b, Θ_s = polar angles of body and shock surfaces, respectively
Θ_0 = strained polar angle
σ = β/δ
ϕ_ℓ = dihedral angle in base plane

Introduction

NONCIRCULAR body cross sections and various lifting-body configurations are of current interest as a means for obtaining long-range and high-performance supersonic missile characteristics. Configurations based on half-cones with delta-wing flat tops were advanced by Eggers[1] in 1960 for high-altitude long-range hypersonic flight. Configurations based on caret waveriders were also advanced in the early 1960s owing to their simple known two-dimensional-based flowfields. A general discussion of these types of configurations is presented by Küchemann,[2] and related discussions are given by Townend[3] and Stollery.[4]

Recently, lifting-body configurations derived from cone flowfields[5-8] or derived from sections of cones[9] have received attention. Various effects on performance stemming from Mach number variations, geometry variations, optimization,[10] and viscous drag[11] have been ascertained. Whereas the conical bodies and their associated conical flowfields have proved very useful and enlightening for parametric design studies, the sharp-nosed conical bodies themselves are not particularly advantageous for the packaging of guidance, propulsion, and payload units. In this regard, bodies with a more ogival shape, i.e., with longitudinal curvature, are more advantageous for packaging purposes. Moreover, for the same initial nose angle, it is possible that the lift-to-drag ratio can be increased for waveriders with longitudinal curvature derived from a perturbation of the conical waveriders. The purpose of this paper is to address longitudinal curvature on these cone-derived waverider configurations and to establish some general results associated with parameter variations.

Formulation of the Problem

The starting configuration of basic interest is the idealized-cone waverider, shown in Fig. 1a. This configuration is a limiting case of more complicated and realistic shapes,[5,6,10] such as the elliptic-cone waverider shown in Fig. 1b, and it lends itself to a simple analysis while still exemplifying more general configurations. The effects of longitudinal curvature are accounted for by a perturbation of the axisymmetric flow past a circular cone, the basis of which is sketched in Fig. 2. Conventional spherical polar coordinates r, Θ, and ϕ are used in the analysis. Since the development is axisymmetric, the azimuthal angle ϕ does not appear, except for the dihedral angle ϕ_ℓ of the final waverider configuration. The basic-cone body is perturbed by the relation

$$\Theta_b = \delta[1 - \epsilon f(r/\ell)] \tag{1}$$

where δ is the basic-cone angle, $f(r/\ell)$ a prescribed function that produces the longitudinal curvature, ℓ the length of the body, and ϵ a small perturbation parameter being essentially the ratio of the body length over the initial radius of curvature of the body. The corresponding shock shape is given by

$$\Theta_s = \delta[\sigma - \epsilon g(r/\ell)] \tag{2}$$

where $g(r/\ell)$ is a function determined by the analysis and $\sigma \equiv \beta/\delta$ the shock-to-body angle ratio of the basic problem. The perturbation analysis for this problem has already been carried out,[12] and the results for the flowfield are available for our utilization. A modified synopsis of this analysis will be presented herein, and the nature of the shock-layer structure described.

When the perturbed body, shock, and flowfield are used to construct a perturbation to the idealized cone waverider,

Presented as Paper 84-2100 at the AIAA Atmospheric Flight Mechanics Conference, Seattle, WA, Aug. 21-23, 1984; received March 21, 1985; revision received Oct. 7, 1985.

*Professor, School of Aerospace, Mechanical, and Nuclear Engineering. Associate Fellow AIAA.
†Graduate Student, School of Aerospace, Mechanical and Nuclear Engineering.

the resulting waverider configuration is as shown in Fig. 3. The leading edges of the waverider winglets are now curved instead of straight as for the unperturbed waverider shown in Fig. 1a.

The flowfield outside the viscous boundary layer is governed by the mass, momentum, and energy equations for steady inviscid isentropic flow, i.e,

$$\text{div}\rho V = 0 \tag{3a}$$

$$\rho V \cdot \nabla V = -\nabla p \tag{3b}$$

$$V \cdot \nabla s = 0 \tag{3c}$$

where V is the velocity vector, and ρ, p, and s are the density, pressure, and specific entropy, respectively. In addition, we have the equation of state for a thermally and calorically perfect gas:

$$\frac{s-s_0}{c_v} = \ell n\left(\frac{p}{p_0}\right) - \gamma \ell n\left(\frac{\rho}{\rho_0}\right) \tag{3d}$$

where c_v and c_p are specific heats at constant volume and pressure, $\gamma \equiv c_p/c_v$, and s_0, p_0, and ρ_0 are suitable reference quantities. It is convenient to utilize the compressible Bernoulli equation

$$\frac{\gamma p}{(\gamma-1)\rho} + \frac{V^2}{2} = \text{const} \tag{3e}$$

which is not independent of Eqs. (3a-d), but a statement that the total enthalpy is conserved throughout the flow.

Owing to the nonanalytic behavior of the perturbation variables at the body surface, it is useful, and, in fact, necessary to introduce a new independent variable $\Theta_0 = \Theta_0(\Theta, r)$ that is tantamount to a straining of the geometric polar angle Θ between the body and the shock. It is convenient to define Θ_0 such that

$$\frac{\Theta_0 - \delta}{\beta - \delta} \equiv \frac{\Theta - \Theta_b}{\Theta_s - \Theta_b} \tag{4}$$

Thus, Θ_0 takes the constant values δ and β at the perturbed body and shock, whereas Θ takes the values δ and β at the unperturbed basic body and basic shock. The new independent variables are thus (Θ_0, r) which replace (Θ, r).

Perturbation Expansions

As shown in Ref. 12, the independent variables become separable when the body perturbation $f(r/\ell)$ has the power-series form

$$\epsilon f\left(\frac{r}{\ell}\right) = \sum_{m>0} \epsilon_m \left(\frac{r}{\ell}\right)^m \tag{5}$$

where the ϵ_m's are all of the same order of smallness as ϵ. The corresponding shock function $g(r/\ell)$ will then have the form

$$\epsilon g\left(\frac{r}{\ell}\right) = \sum_{m>0} \epsilon_m \left(\frac{r}{\ell}\right)^m G_m \tag{6}$$

where the values of G_m, for each value of m, are to be determined from the analysis. With these expansions, we now get from Eq. (4) the perturbation transformation

$$\Theta = \Theta_0 + \sum_{m>0} \epsilon_m \left(\frac{r}{\ell}\right)^m \Theta_m \tag{7a}$$

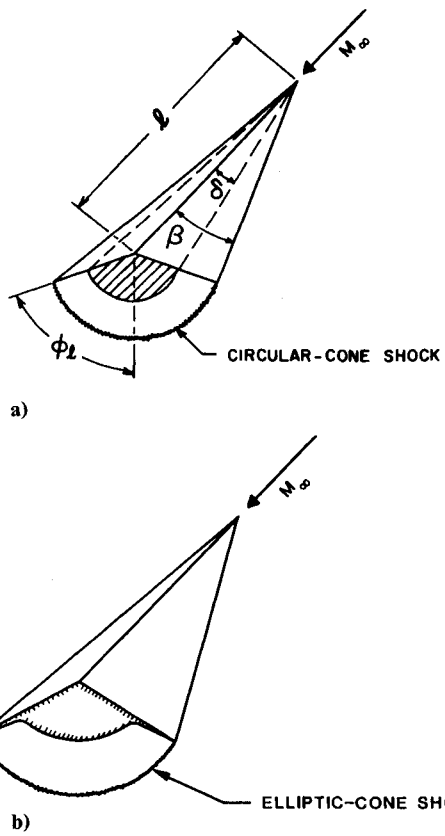

Fig. 1 Cone-derived waveriders: a) idealized waverider, b) elliptic-cone waverider.

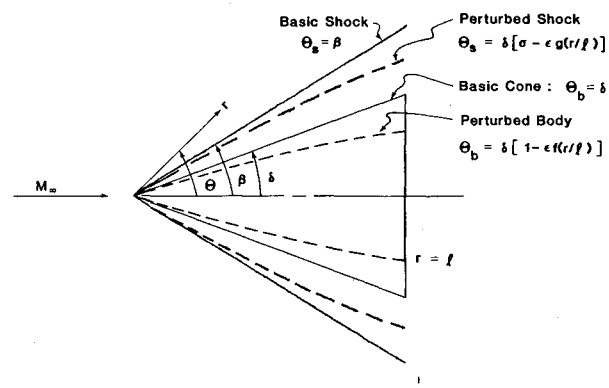

Fig. 2 Ogival body produced by perturbatiqn of a cone.

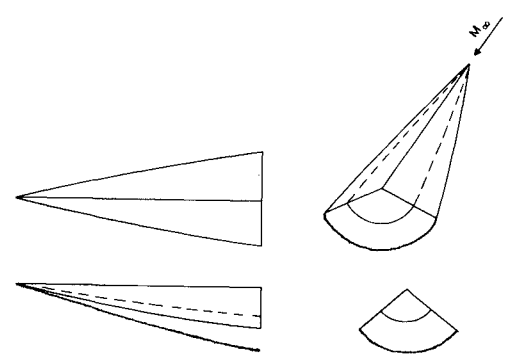

Fig. 3 Idealized cone-derived waverider with longitudinal curvature.

where

$$\Theta_m \equiv \delta\left[(1-G_m)\frac{\Theta_0-\delta}{\beta-\delta}-1\right] \tag{7b}$$

The perturbed flowfield differs only slightly from the conical flow past a circular cone. Thus, we assume the first-order expansions

$$u(\Theta,r)=u_0(\Theta_0)+\sum_{m>0}\epsilon_m\left(\frac{r}{\ell}\right)^m U_m(\Theta_0)+\mathcal{O}(\epsilon^2) \tag{8a}$$

$$v(\Theta,r)=v_0(\Theta_0)+\sum_{m>0}\epsilon_m\left(\frac{r}{\ell}\right)^m V_m(\Theta_0)+\mathcal{O}(\epsilon^2) \tag{8b}$$

$$p(\Theta,r)=p_0(\Theta_0)\left[1+\sum_{m>0}\epsilon_m\left(\frac{r}{\ell}\right)^m P_m(\Theta_0)+\mathcal{O}(\epsilon^2)\right] \tag{8c}$$

$$\rho(\Theta,r)=\rho_0(\Theta_0)\left[1+\sum_{m>0}\epsilon_m\left(\frac{r}{\ell}\right)^m R_m(\Theta_0)+\mathcal{O}(\epsilon^2)\right] \tag{8d}$$

$$s(\Theta,r)=s_0+c_v\sum_{m>0}\epsilon_m\left(\frac{r}{\ell}\right)^m S_m(\Theta_0)+\mathcal{O}(\epsilon^2) \tag{8e}$$

where

$$V=u\vec{e}_r+v\vec{e}_\Theta \tag{8f}$$

These expansions are essentially the same as in Ref. 12, except that we have utilized the entropy variable and the straining transformation, Eq. (7). The details of the subsequent modified analysis can be found in Ref. 13.

The basic conical-flow variables u_0, v_0, ρ_0, p_0, and s_0 can be obtained from well-known tabulations. Our purposes are facilitated by using accurate approximations that have proved useful in similar perturbation analyses[10,12]:

$$u_0(\Theta_0)\simeq V_\infty\left[1-\frac{\delta^2}{2}\left(\frac{\Theta^2}{\delta^2}+\ell n\frac{\beta^2}{\Theta_0^2}\right)\right] \tag{9a}$$

$$v_0(\Theta_0)\simeq -V_\infty\Theta_0\left(1-\frac{\delta^2}{\Theta_0^2}\right) \tag{9b}$$

$$\frac{a_0^2(\Theta_0)}{a_\infty^2}\equiv T_0(\Theta_0)/T_\infty\simeq 1+\frac{\gamma-1}{2}K_\delta^2\left[2-\frac{\delta^2}{\Theta_0^2}+\ell n\frac{\beta^2}{\Theta_0^2}\right] \tag{9c}$$

$$p_0(\Theta_0)/p_\infty\simeq 1+\frac{\gamma}{2}K_\delta^2\left[1+\frac{\rho_0(\beta)}{\rho_\infty}\left(1-\frac{\delta^2}{\Theta_0^2}+\ell n\frac{\beta^2}{\Theta_0^2}\right)\right] \tag{9d}$$

$$\rho_0(\Theta_0)/\rho_\infty=\frac{p_0(\Theta_0)/p_\infty}{T_0(\Theta_0)/T_\infty}\simeq\frac{\rho_0(\beta)}{\rho_\infty}\left[1+\frac{K_\delta^2}{2(T_0(\beta)/T_\infty)}\times\left(\frac{\delta^2}{\beta^2}-\frac{\delta^2}{\Theta_0^2}+\ell n\frac{\beta^2}{\Theta_0^2}\right)\right] \tag{9e}$$

where

$$\xi_0\equiv\frac{\rho_\infty}{\rho_0(\beta)}\simeq 1-\frac{1}{\sigma^2} \tag{9f}$$

and

$$\sigma\equiv\frac{\beta}{\delta}\simeq\left[\frac{\gamma+1}{2}+\frac{1}{K_\delta^2}\right]^{1/2} \tag{9g}$$

These approximations are valid for small cone angles and large Mach numbers within the framework of hypersonic small-disturbance theory. The hypersonic similarity variable is $K_\delta\equiv M_\infty\delta$. The hypersonic small-disturbance approximation will be continued in the subsequent analysis.

The boundary conditions on the body surface, $\Theta=\Theta_b$ or $\Theta_0=\delta$, are described by the tangency condition $V\cdot\hat{n}_b=0$. For the perturbation variables, the tangency condition reduces to

$$v_0(\delta)=0 \quad \text{and} \quad V_m(\delta)=-m\delta V_\infty \tag{10}$$

At the shock, $\Theta=\Theta_s$ or $\Theta_0=\beta$, the usual gasdynamic jump conditions lead to

$$u_0(\beta)=V_\infty\cos\beta\simeq V_\infty \tag{11a}$$

$$U_m(\beta)\simeq\delta^2 V_\infty\sigma G_m\left[1+\frac{m}{\sigma^2}\right] \tag{11b}$$

$$v_0(\beta)=-V_\infty\xi_0\sin\beta\simeq-\delta V_\infty\sigma\xi_0 \tag{11c}$$

$$V_m(\beta)\simeq\delta V_\infty G_m\left[(1+m)\left\{\frac{2(\gamma-1)}{\gamma+1}-\xi_0\right\}-m\right] \tag{11d}$$

$$s_0(\beta)=s_\infty+c_v\left[\ell n\frac{p_0(\beta)}{p_\infty}+\gamma\ell n\xi_0\right] \tag{11e}$$

$$S_m(\beta)\cong-\frac{\gamma(\gamma-1)}{a_0^2(\beta)/a_\infty^2}\frac{K_\delta^2 G_m(1+m)}{\sigma^3} \tag{11f}$$

where $a_0^2\equiv\gamma p_0/\rho_0=\gamma RT_0$ is the square of the speed of sound in the basic flow. The other variables at the shock can be determined in terms of Eqs. (11).

Analysis

Basic Procedure

When the expansions [Eqs. (7) and (8)] are substituted into the governing equations, it is found that the first-order perturbation equations are equidimensional in r and, hence, that the Θ_0 dependencies can be sorted out for each order of m individually.[12,13] Then, the state variables can be expressed as functions of the velocity components until, finally, a single ordinary equation for U_m can be obtained. When the solution for U_m is obtained, all of the other variables are also determined, since they can be expressed as functions of U_m.

The development of the solution can be started with energy equation (3c). Making use of the zeroth-order continuity equation, we can establish that the first-order entropy perturbations $S_m(\Theta_0)$ have the form

$$S_m(\Theta_0)=S_m(\beta)\left[\frac{\rho_0(\Theta_0)v_0(\Theta_0)\sin\Theta_0}{\rho_0(\beta)v_0(\beta)\sin\beta}\right]^{m/2} \tag{12a}$$

$$\simeq S_m(\beta)\left[\frac{\Theta_0^2-\delta^2}{\beta^2-\delta^2}\right]^{m/2} \tag{12b}$$

Expression (12a) is exact, and expression (12b) is the hypersonic small-disturbance approximation that is consistent with Eqs. (9) [since $\rho_0(\Theta_0)/\rho_0(\beta)\simeq 1$]. The entropy perturbations vanish on the body surface, since the streamlines that wet the body surface pass through the shock at its vertex, where the perturbations vanish. The value at the shock $S_m(\beta)$ contains the shock parameter G_m which remains to be determined. The functions [Eqs. (12)] show the nonanalytic character of the solution at the body surface.

The equation of state [Eq. (3d)] and the compressible Bernoulli equation [Eq. (3e)] are algebraic, and the first-order perturbations for P_m and R_m can be sorted out and written in the form

$$P_m=-\gamma(u_0U_m+v_0V_m)/a_0^2-S_m/(\gamma-1) \tag{13a}$$

$$R_m=-(u_0U_m+v_0V_m)/a_0^2-S_m/(\gamma-1) \tag{13b}$$

The velocity functions U_m and V_m remain to be determined from the mass and r-momentum perturbation equations.

Now the remaining equations can be simplified if we introduce new velocity variables U_m^* and V_m^* such that

$$U_m = U_m^* + \Theta_m v_0 \tag{14a}$$

$$V_m = V_m^* + \Theta_m \frac{dv_0}{d\Theta_0} \tag{14b}$$

The functions U_m^* *and* V_m^* are essentially the velocity functions occurring in Ref. 12 with Θ as the independent variable. They are related to U_m and V_m by reconciliation of the perturbation expansions [Eqs. (8a) and (8b)] with the straining transformation [Eqs. (7a)]. In terms of the new variables, the r component of the momentum equation (3b) generates V_m^* as a function of U_m^*:

$$V_m = \frac{1}{1+m}\left[\frac{dU_m^*}{d\Theta_0} - \frac{ma_0^2 S_m}{\gamma(\gamma-1)v_0}\right] \tag{15}$$

The analysis of Ref. 12 can be simplified if a further transformation function U_m^{**} is introduced such that

$$U_m^{**} = U_m^* - \int_\delta^{\Theta_0} \frac{ma_0^2 S_m d\Theta_0}{\gamma(\gamma-1)v_0} \tag{16}$$

It follows that

$$V_m^* = \frac{1}{1+m}\frac{dU_m^{**}}{d\Theta_0} \tag{17}$$

When the foregoing results are used in the first-order perturbation of the continuity equation (3a), a single equation for U_m^{**} can be obtained:

$$(1-A)\frac{d^2U_m^{**}}{d\Theta_0^2} + \left[(1-B)\cot\Theta_0 - \frac{2mu_0v_0}{a_0^2}\right]\frac{dU_m^{**}}{d\Theta_0} + (1+m)\left[2-C+m\left(1-\frac{u_0^2}{a_0^2}\right)\right]U_m^{**} = H_m(\Theta_0) \tag{18}$$

where

$$A(\Theta_0) \equiv v_0^2/a_0^2 \tag{19a}$$

$$B(\Theta_0) \equiv \left[\frac{v_0}{a_0^2}(u_0+v_0') - \frac{d\ell n\rho_0}{d\Theta_0} - \frac{v_0^2}{a_0^2}\frac{d\ell n a_0^2}{d\Theta_0}\right]\tan\Theta_0 \tag{19b}$$

$$C(\Theta_0) \equiv \frac{v_0^2}{a_0^2} - \frac{u_0v_0}{a_0^2}\frac{d\ell n a_0^2}{d\Theta_0} \tag{19c}$$

$$H_m(\Theta_0) \equiv \frac{m(1+m)}{\gamma(\gamma-1)}\left[u_0S_m - \left\{2-C+m\left(1-\frac{u_0^2}{a_0^2}\right)\right\}\int_\delta^{\Theta_0}\frac{a_0^2S_m}{v_0}d\Theta_0\right] \tag{19d}$$

Approximate Solution

Approximations utilized previously for analogous problems[5,10,12] have shown how accurate approximate solutions to equations of the type of Eq. (18) can be obtained. We shall adopt these herein. At the body surface, v_0 and S_m vanish, and hence A, B, C, and H_m vanish at the body surface. Further, ρ_0 and a_0 vary slowly across the shock layer and hence can be regarded approximately as constants. Thus, we set A, B, and C equal to zero approximately, and also the coefficient $2mu_0v_0/a_0^2$ of $dU_m^*/d\Theta_0$ as well. If a_0^2 is treated as a constant in the integral appearing in H_m, then by means of Eqs. (9b) and (12b), we can evaluate H_m as

$$H_m(\Theta_0) \simeq \frac{(1+m)}{\gamma(\gamma-1)}(2+m-C)\frac{a_0^2S_m}{u_0} \tag{20}$$

Finally, we note that δ and Θ_0 are small angles and, thus, in the hypersonic small-disturbance approximation, we have

$$\frac{u_0^2}{a_0^2} \simeq \frac{K_\delta^2}{a_0^2(\beta)/a_\infty^2}\frac{1}{\delta^2} \tag{21}$$

Thus, the factor $2+m-C$ appearing as a coefficient of U_m^{**} is negligible in the hypersonic small-disturbance approximation, as well as the function H_m. The embryonic form of Eq. (18) is thus simply

$$\frac{d^2U_m^{**}}{d\Theta_0^2} + \frac{1}{\Theta_0}\frac{dU_m^{**}}{d\Theta_0} - \frac{\lambda_m^2}{\delta^2}U_m^{**} = 0 \tag{22}$$

where

$$\lambda_m \equiv \left[\frac{m(1+m)K_\delta^2}{a_0^2(\beta)/a_\infty^2}\right]^{1/2} \tag{23}$$

The solution to Eq. (22) is

$$\frac{U_m^{**}(\Theta_0)}{\delta^2 V_\infty} = (1+m)G_m[A^*I_0(\lambda_m z) + B^*K_0(\lambda_m z)] \tag{24}$$

where $z \equiv \Theta_0/\delta$, I_0 and K_0 are the modified Bessel functions of the first and second kinds, A^* and B^* are constants of integration, and where we have anticipated certain functional dependencies. When the integral in Eq. (16) is evaluated approximately, as for the function H_m given by Eq. (20), the expressions for U_m^* and V_m^* from Eqs. (16) and (17) become

$$\frac{U_m^*(\Theta_0)}{\delta^2 V_\infty} = (1+m)G_m\left[A^*I_0(\lambda_m z) + B^*K_0(\lambda_m z) + \frac{1}{\sigma^3}\left(\frac{z^2-1}{\sigma^2-1}\right)^{m/2}\right] \tag{25a}$$

$$\frac{V_m^*(\Theta_0)}{\delta V_\infty} = \lambda_m G_m[A^*I_1(\lambda_m z) - B^*K_1(\lambda_m z)] \tag{25b}$$

The shock conditions [Eqs. (11b) and (11d)] and the surface tangency condition [Eq. (10)] constitute three boundary conditions for determining A^*, B^*, and G_m [by means of Eqs. (14)]. We evaluate $dv_0/d\Theta_0$ from the exact basic-flow equation[13]

$$\left(1-\frac{v_0^2}{a_0^2}\right)\frac{dv_0}{d\Theta_0} + \cot\Theta_0 v_0 + \left(2-\frac{v_0^2}{a_0^2}\right)u_0 = 0 \tag{26}$$

Using Eqs. (9a) and (9b) for u_0 and v_0, and evaluating a_0^2 at the shock by means of Eq. (9c), we solve for $dv_0/d\Theta_0$ and obtain the hypersonic small-disturbance form

$$\frac{1}{V_\infty}\frac{dv_0}{d\Theta_0} = -\left(1+\frac{1}{z^2}\right) - \frac{W(z)}{z^2(1-W(z))} \tag{27a}$$

where

$$W(z) \equiv \frac{v_0^2(z)}{a_0^2(\beta)} = \frac{K_\delta^2}{a_0^2(\beta)/a_\infty^2}\left(z-\frac{1}{z}\right)^2 \tag{27b}$$

Imposing the shock conditions [Eqs. (11b) and (11d)] now leads to the evaluation of A^* and B^*:

$$A^* = \sigma\lambda_m[C^*K_1(\lambda_m\sigma) + D^*K_0(\lambda_m\sigma)] \tag{28a}$$

$$B^* = \sigma\lambda_m [C^* I_1(\lambda_m\sigma) - D^* I_0(\lambda_m\sigma)] \tag{28b}$$

where

$$C^* \equiv \frac{1}{\sigma} - \frac{1}{\sigma^3} \tag{28c}$$

$$D^* \equiv \frac{1}{\lambda_m}\left[\frac{m}{\sigma^2} - \frac{4(1+m)}{\gamma+1} - \frac{W(\sigma)}{\sigma^2\{1-W(\sigma)\}}\right] \tag{28d}$$

Imposing the surface tangency condition [Eq. (10)] leads to the value of the shock-perturbation factor

$$G_m = \frac{2+m}{\lambda_m [B^* K_1(\lambda_m) - A^* I_1(\lambda_m)]} \tag{29}$$

The first-order solution is now complete, and the entire shock-layer flowfield can be computed. The results are essentially the same as in Ref. 12, but the present procedure is somewhat different. Moreover, the results are in terms of the strained variable Θ_0 which describes the flowfield between the perturbed body and perturbed shock, rather than in terms of Θ as for Ref. 12 which describes the flowfield between the *unperturbed* body and *unperturbed* shock. The present analysis is more appropriate for constructing waverider configurations from the known flowfield.

Shock-Layer Structure

The validity of the foregoing approximate analysis can be established by comparison of some of the results with the numerical results of Van Dyke.[14] Figure 4 shows the shock-perturbation factor G_m as a function of $K_\delta \equiv M_\infty \delta$ for $m = 1$, 2, 3. The points with circles and squares are the discrete results from Ref. 14. For $m = 1$, the present results agree well with the numerical calculations of Van Dyke,[14] being slightly higher for K_δ less than 1. The present results for $m = 2$ are slightly higher than the three discrete points computed by Van Dyke. As m increases, the value of G_m decreases. Since G_m is always less than unity, the perturbation of the shock location is always less than the corresponding perturbation of the body location.

Another comparison can be made with the body-surface perturbation pressure coefficient, defined as

$$\frac{C_{p_m}(\delta)}{\delta^2} = \frac{2p_0(\delta)P_m(\delta)}{\gamma p_\infty K_\delta^2} \tag{30}$$

In the evaluation shown in Fig. 5, $p_0(\delta)$ was replaced by the shock value $p_0(\beta)$ [from Eq. (9d)], since this gave more accurate results and is not inconsistent with the constant-density or slowly varying properties of the basic-cone shock layer. The values of $m = 1$ compare well with Van Dyke,[14] being slightly higher for $K_\delta < 1$. For $m = 2$, the present results are slightly higher (more negative) than the four discrete points from Van Dyke. The perturbation pressure coefficient is negative, and becomes more negative as m increases, since the ogival shape for positive ϵ produces a flow expansion.

Figure 6 shows the radial velocity perturbations U_1 and U_2 as a function of Θ_0 across the shock layer for various values of K_δ. These perturbations are positive and approach a hypersonic limit as K_δ becomes large, where they show small variations across the shock layer. Figure 7 shows the polar velocity perturbations V_1 and V_2 across the shock layer for various values of K_δ. The polar perturbations are negative (toward the body) and nearly have obtained the hypersonic limit at $K_\delta = 5$. The pressure perturbations P_1 and P_2 are shown in Fig. 8. The perturbations for $m = 1$ and 2 are very similar, being greater at the body than at the shock. For large values of K_δ, the perturbations are fairly large, the more so for larger m, so that even where ϵ is fairly small the total perturbation ϵP_m may be significant. The density perturbations R_1 and R_2 are shown in Fig. 9. Because the shock-layer flow is expanding (for positive ϵ), the density perturbations are negative and greater at the body than at the shock. In the hypersonic limit $K_\delta = \infty$, the density perturbations at the shock are zero, since the limiting density ratio across the shock $(\gamma+1)/(\gamma-1)$ is accounted for entirely by the basic-cone solution (zeroth-order approximation). The entropy perturbation S_1 is illustrated in Fig. 10. Whereas the entropy perturbations at the shock are negative because the perturbed shock is weaker than the basic shock (for $\epsilon > 0$), they vanish at the body because the surface streamlines pass through the vertex of the shock which is essentially unperturbed for $m > 0$. As Eqs. (12) indicate, the entropy perturbations at the body $\Theta_0 = \delta$ are nonanalytic for odd positive values of m.

Waverider Configurations

When the velocity field is known, stream surfaces can be established in the shock layer, and from these waverider lifting-body configurations can be constructed.[5,10] A general optimization analysis analogous to that of Ref. 10 for axisymmetric conical flow could be performed, but we shall be concerned here with the special simple limiting case of the idealized waverider.

Since the flow is axisymmetric, any plane passing through the axis of symmetry is a stream surface. The body surface is

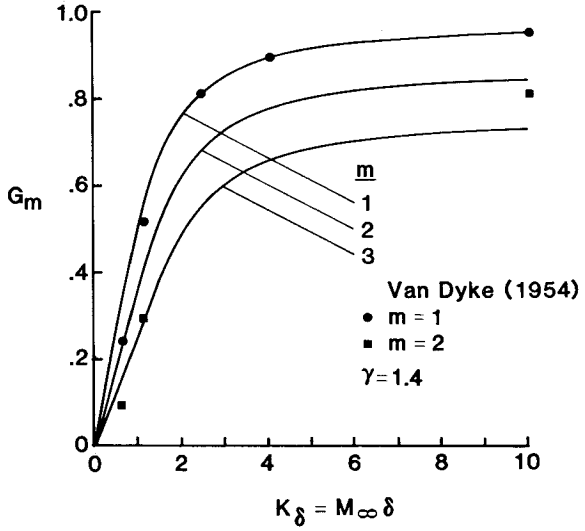

Fig. 4 Shock-perturbation factor G_m vs K_δ.

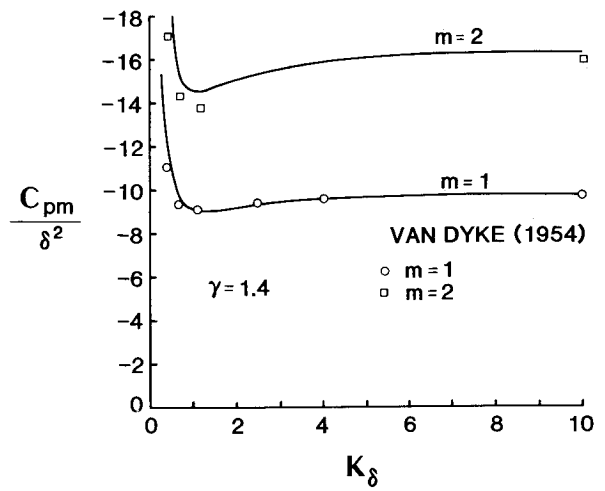

Fig. 5 Surface perturbation pressure coefficient vs K_δ.

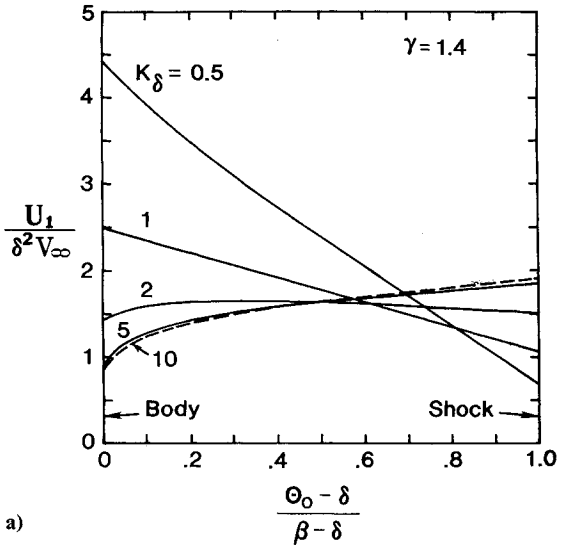

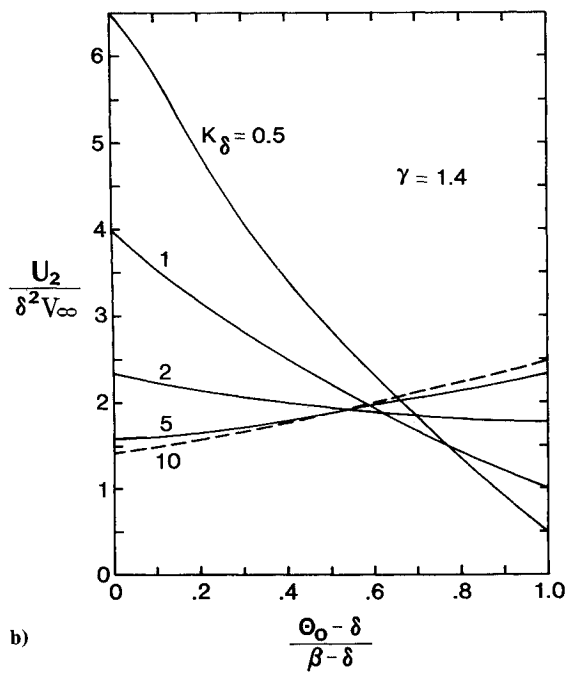

Fig. 6 Variation of radial velocity perturbation across shock layers, a) $m=1$, b) $m=2$.

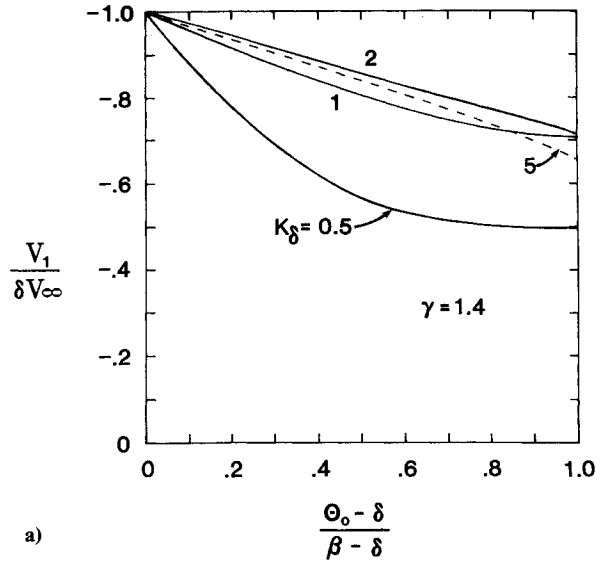

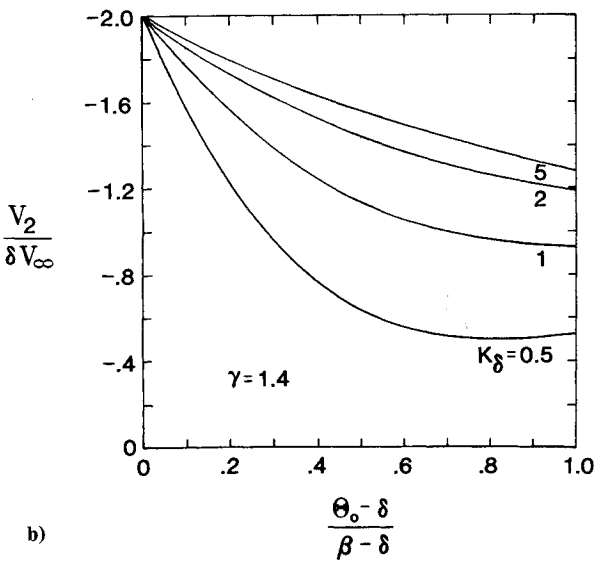

Fig. 7 Variation of polar velocity perturbation across shock layers, a) $m=1$, b) $m=2$.

also a stream surface. We can thus construct a lifting-body configuration by selecting a pair of planes passing through the axis of symmetry, oriented at a dihedral angle ϕ_ℓ as shown in Fig. 1a, and acting as infinitesimally thin winglets. On the top surface the shock-disturbed flowfield is discarded in favor of the undisturbed freestream flow. On the lower compression surface the plane surface extends as a winglet from the shock to the ogival body, and the remainder of the compression surface is the ogival body itself. The resulting body thus appears to be riding on an ogival shock wave attached beneath it, such as shown in Fig. 3. This idealized configuration is a limiting case of more general configurations having finite-thickness winglets that blend into the body, analogous to the conical configuration shown in Fig. 1b.

Since the pressure in the shock layer, and thus on the stream surface, is known, the lift and wave drag can be computed by direct integration of the pressure over the body surface. Since the winglets are aligned with the freestream, they produce no wave drag. The pressure perturbation on the winglets depends on both r and Θ. For the lift, the r integration is simply carried out leaving only a quadrature over Θ_0 for the perturbation contribution. The wave drag comes entirely from the ogival-body on which the pressure varies only with r and yields to a simple integration. Thus, the lift and wave drag take the forms

$$L = L_0\left[1 + \sum_{m>0} \epsilon_m L_m\right] \tag{31}$$

$$D_w = D_0\left[1 + \sum_{m>0} \epsilon_m D_m\right] \tag{32}$$

The contributions from the unperturbed idealized cone-derived waverider have been obtained previously[6,10] and are

$$L_0 \equiv q\ell^2 \frac{\sigma^2\delta^3}{\sigma+1}\sin\phi_\ell \tag{33a}$$

$$D_0 \equiv q\ell^2\delta^2 C_{p_0}(\delta)\phi_\ell \tag{33b}$$

where $q \equiv \rho_\infty V_\infty^2/2$, and

$$\frac{C_{p_0}(\delta)}{\delta^2} = 1 + \frac{\sigma^2 \ell n \sigma^2}{\sigma^2 - 1} \tag{33c}$$

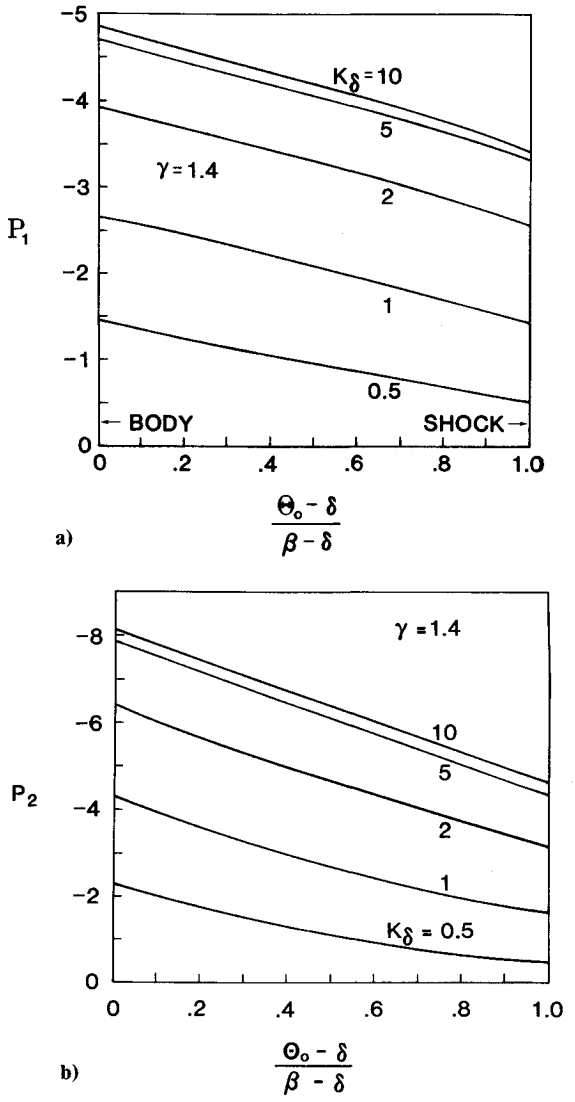

Fig. 8 Variation of pressure perturbation across shock layers, a) $m=1$, b) $m=2$.

The perturbation contributions from longitudinal curvature depend on K_δ and m only and are

$$L_m \equiv \frac{\sigma+1}{2(2+m)\sigma^2}\left[\frac{4\sigma^2}{\sigma+1}\frac{d\Theta_m}{d\Theta_0} - \left(1+\frac{d\Theta_m}{d\Theta_0}\right)\frac{C_{p_0}(\delta)}{\delta^2} + \frac{C_{p_m}(\delta)}{\delta^2} + \int_1^\sigma \frac{C_{p_m}(z)}{\delta^2}dz\right] \tag{34a}$$

$$D_m \equiv \frac{2}{2+m}\frac{C_{p_m}(\delta)}{C_{p_0}(\delta)} - 2 \tag{34b}$$

where

$$\frac{d\Theta_m}{d\Theta_0} = \frac{1-G_m}{\sigma-1} \tag{34c}$$

and C_{p_m} is computed from Eq. (30) with $p_0(z)$ evaluated at the shock value, $p_0(\beta)$, consistent with the calculation of Fig. 5. The base drag has been omitted, which is tantamount to setting the base pressure equal to p_∞.

The perturbations for $m=1$ and 2 are shown in Fig. 11 as functions of K_δ. Both the lift and drag contributions are negative, becoming larger negative for larger values of K_δ. The perturbations become larger as m increases. The effect of

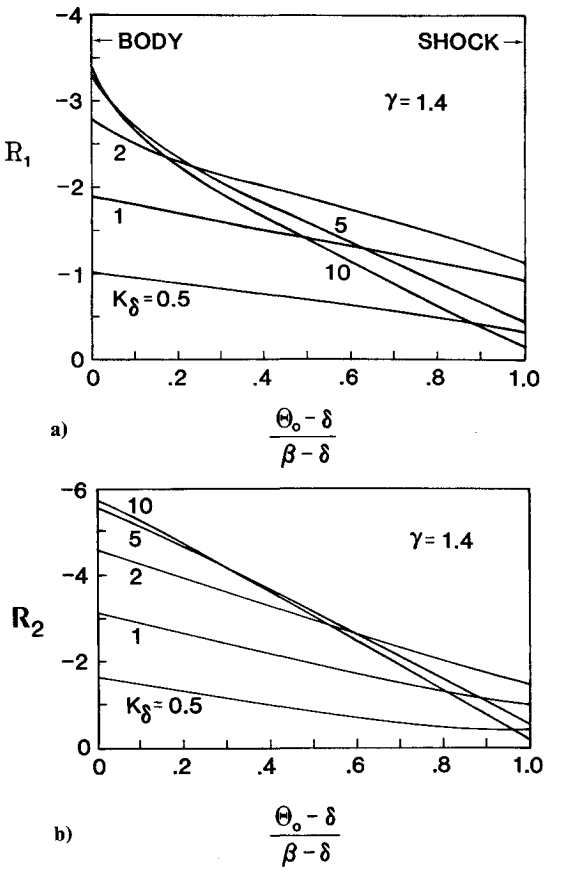

Fig. 9 Variation of density perturbation across shock layers, a) $m=1$, b) $m=2$.

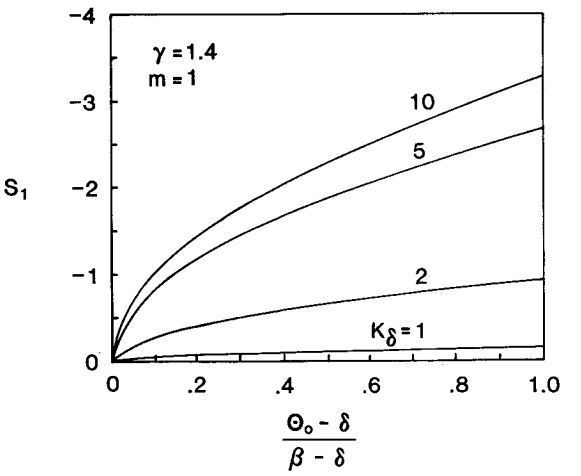

Fig. 10 Variation of entropy perturbation across shock layer, a) $m=1$.

longitudinal curvature is thus to reduce both the lift and wave drag, the more so for the larger value of m. The drag, however, is reduced more than the lift, and hence the lift-to-drag ratio is actually increased. For small values of ϵ, we have

$$\frac{L}{D_w} = \frac{L_0}{D_0}\left[1 + \sum_{m>0}\epsilon_m(L_m - D_m) + \mathcal{O}(\epsilon^2)\right] \tag{35}$$

The perturbations in the inviscid lift-to-drag ration, $L_m - D_m$, are also shown in Fig. 11 for $m=1$ and 2.

If the magnitude of the perturbation is such as to reduce the base radius by 10% then $\epsilon = 0.1$. If $K_\delta = 3$ and $m=1$, then the

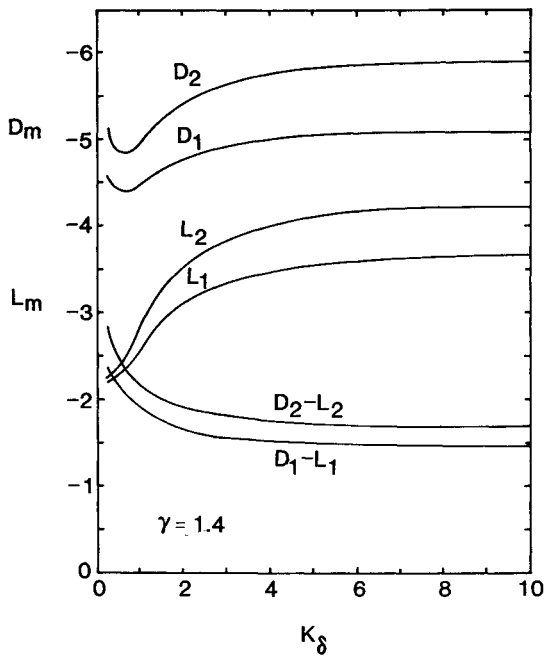

Fig. 11 Longitudinal-curvature lift and drag perturbations vs K_δ for idealized cone-derived waverider.

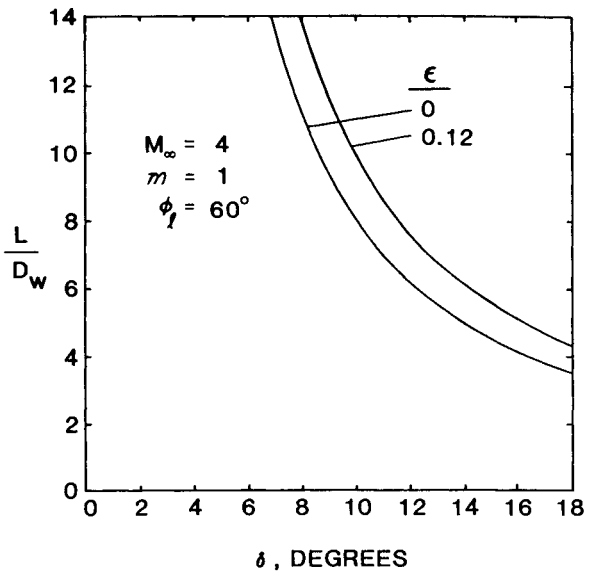

Fig. 12 Lift-to-drag ratio as a function of cone angle for $\epsilon = 0$ and 0.12.

forebody wave drag is reduced by 49%, the lift by 33.5%, and the inviscid lift-to-drag ratio increases by 15.5% [according to the first-order correction, Eq. (35), which is probably conservative].

The effect of longitudinal curvature on the inviscid lift-to-drag ratio is shown in Fig. 12, according to Eq. (35). In this figure, L/D_w is plotted as a function of the unperturbed cone angle δ for $M_\infty = 4$ and $m = 1$. The curve for the unperturbed idealized waverider is represented by $\epsilon = 0$, and the curve for longitudinal curvature is shown for $\epsilon = 0.12$. This figure illustrates the dramatic improvement in the inviscid lift-to-drag ratio produced by longitudinal curvature. One may also verify from this figure that a waverider without longitudinal curvature having the same slenderness ratio as a waverider with longitudinal curvature, that is, with a reduced cone angle given by $\delta_r = \delta(1-\epsilon)$, has a smaller lift-to-drag ratio than its counterpart with longitudinal curvature.

Effect of Longitudinal Curvature on Design Parameters

Missile and aircraft design considerations involve such factors as base area A_b, volume V, projected planform area S, and forebody wetted area S_w. For the idealized cone-derived waverider without longitudinal curvature, such as shown in Fig. 1a, these factors are found to be[6,10,11]

$$A_{b_0} = \ell^2\delta^2\phi_\ell \tag{36a}$$

$$V_0 = \ell^3\delta^2\phi_\ell/3 \tag{36b}$$

$$S_0 = \ell^2\delta\sigma\sin\phi_\ell \tag{36c}$$

$$S_{w_0} = \ell^2\delta[2\sigma + \phi_\ell - 1] \tag{36d}$$

By a straightforward use of geometry and calculus, the corresponding first-order results for small longitudinal curvature are

$$A_b = A_{b_0}[1-2\epsilon] \tag{37a}$$

$$V = V_0\left[1 - \frac{6\epsilon}{m+3}\right] \tag{37b}$$

$$S = S_0\left[1 - \frac{2G_m\epsilon}{\sigma(2+m)}\right] \tag{37c}$$

$$S_w = S_{w_0}\left[1 - \frac{2(\phi_\ell + 2G_m - 1)\epsilon}{(2+m)(2\sigma+\phi_\ell-1)}\right] \tag{37d}$$

Another factor of importance is the ratio $V^{2/3}/S$, for which we have to first order

$$\frac{V^{2/3}}{S} = \frac{V_0^{2/3}}{S_0}\left[1 - \left\{\frac{4}{m+3} - \frac{2G_m}{\sigma(2+m)}\right\}\epsilon\right] \tag{38}$$

Again, we note that when $\epsilon = 0.1$, $K_\delta = 3$, and $m = 1$ the base area is reduced by 20%, the volume by 15%, the projected planform area by 5%, and the ratio $V^{2/3}/S$ by 5%. If the dihedral angle ϕ_ℓ is 50 deg, the forebody wetted area is reduced by 5%.

Concluding Remarks

The perturbations due to longitudinal curvature have their greatest effects on the decrease of wave drag, which, of course, is a primary factor in high-speed missile aerodynamics. The lift is also deceased, but to a lesser degree, and thus the inviscid lift-to-drag ratio shows a modest increase. The preceding formulas allow the total drag

$$D = D_w + D_f + D_b \tag{39}$$

to be estimated. Here, D_f is the friction drag and D_b the base drag. The friction drag can be estimated by the simple formula[11]

$$D_f = qC_fS_w \tag{40}$$

where C_f is an average friction coefficient. If C_f is taken as unchanged by transverse-curvature effects, then D_f decreases a small amount because of the wetted area S_w. The base drag can be expressed as

$$D_b = qC_{p_b}A_b \tag{41}$$

where C_{p_b} is the absolute value of the base pressure coefficient, which in general is difficult to estimate precisely. Because A_b is reduced significantly by transverse curvature, however, then the base drag is also. With these formulas it is

possible to examine the total lift-to-drag ratio over a variety of design conditions, which is worthy of further study.

Transverse curvature reduces the volume from that of the parent conical configuration, but the reduction is mainly in the base region where it is not very useful anyway. Thus, overall, transverse curvature provides a more useful distribution of volume, which is attractive for packaging purposes.

The flowfields shown herein are for the on-design waverider conditions, and thus do not hold for off-design orientations or changes in Mach number. Nevertheless, the on-design flowfield is known accurately and in detail, which is not the case for many other arbitrarily designed missile configurations.

References

[1]Eggers, A.J., "Some Considerations of Aircraft Configurations Suitable for Long-Range Hypersonic Flight," *Hypersonic Flow,* edited by A.R. Coller and J. Tinkler, Butterworths, Washington, DC, 1960, pp. 369-390.

[2]Küchemann, D., *The Aerodynamic Design of Aircraft,* Pergamon Press, London, 1978, Chap. 8.

[3]Townend, L.H., "Research and Design for Lifting Reentry," *Progress in Aerospace and Science,* Vol. 19, No. 1, 1979, pp. 1-180.

[4]Stollery, J.L., "What Has Aerospace Research Led To?," *Aerospace,* Sept. 1982, p. 14.

[5]Rasmussen, M.L., "Waverider Configurations Derived from Inclined Circular and Elliptic Cones," *Journal of Spacecraft and Rockets,* Vol. 17, Nov.-Dec. 1980, pp. 537-545.

[6]Rasmussen, M.L., Jischke, M.C., and Daniel, D.C., "Aerodynamics of Cone-Derived Waverider Missile Configurations," Symposium on Missile Aerodynamics, AGARD CP-336, Trondheim, Norway, Sept. 1982.

[7]Rasmussen, M.L., Jischke, M.C., and Daniel, D.C., "Experimental Forces and Moments on Cone-Derived Waveriders for $M_\infty = 3$ to 5," *Journal of Spacecraft and Rockets,* Vol. 19, Nov.-Dec. 1982, pp. 592-598.

[8]Jischke, M.C., Rasmussen, M.L., and Daniel, D.C., "Experimental Surface Pressures on Cone-Derived Waveriders for $M_\infty = 3$ to 5," *Journal of Spacecraft and Rockets,* Vol. 20, Nov.-Dec. 1983, pp. 539-545.

[9]Schindel, L.H., "Design of High Performance Hypersonic Missiles," AIAA Paper 82-0391, Jan. 1982.

[10]Kim, B.S., Rasmussen, M.L., and Jischke, M.C., "Optimization of Waverider Configurations Generated for Axisymmetic Conical Flow," *Journal of Spacecraft and Rockets,* Vol. 20, Sept.-Oct. 1983, pp. 461-469.

[11]Rasmussen, M.L. and Broadaway, R.T., "Viscous Effects on the Performance of Cone-Derived Waveriders," AIAA Paper 83-2084, Aug. 1983.

[12]Jischke, M.C. and Kim, B.S., "Hypersonic Flow Past an Axisymmetric Body with Small Longitudinal Curvature," *AIAA Journal,* Vol. 20, Oct. 1982, pp. 1346-1351.

[13]Clement, L., "Idealized Cone-Derived Waveriders with Small Longitudinal Curvature," M.S. Thesis, School of Aerospace, Mechanical, and Nuclear Engineering, University of Oklahoma, Norman, OK, July 1984.

[14]Van Dyke, M., "A Study of Hypersonic Small-Disturbance Theory," NACA Rept. 1194, 1954.